Available online at www.sciencedirect.com

ScienceDirect

Physics Procedia 56 (2014) 1208 – 1217

Physics Procedia

8th International Conference on Photonic Technologies LANE 2014

Calibrated Heat Flow Model for Determining the Heat Conduction Losses in Laser Cutting of CFRP

P. Mucha[a,]*, R. Weber[b], N. Speker[a], P. Berger[b], B. Sommer[c], T. Graf[b]

[a]*TRUMPF Laser- und Systemtechnik GmbH, Johann-Maus-Straße 2, 71254 Ditzingen, Germany*
[b]*Institut für Strahlwerkzeuge, University of Stuttgart, Pfaffenwaldring 43, D-70569 Stuttgart, Germany*
[c] *GKN Aerospace Deutschland GmbH, Brunhamstr. 21, 81249 München, Germany*

Abstract

Laser machining has great potential regarding automation in fabrication of CFRP (carbon-fiber-reinforced plastics) parts, due to the nearly force and tool-wear free processing at high process speeds. The high vaporization temperatures and the large heat conductivity of the carbon fibers lead to a large heat transport into the sample. This causes the formation of a heat-affected zone and a decrease of the process speed.

In the present paper, an analytical heat flow model was adapted in order to understand and investigate the heat conduction losses. Thermal sensors were embedded in samples at different distances from the kerf to fit the calculated to the measured temperatures. Heat conduction losses of up to 30% of the laser power were determined. Furthermore, the energy not absorbed by the sample, the energy for sublimating the composite material in the kerf, the energy for the formation of the HAZ, and the residual heat in the sample are compared in an energy balance.

Peer-review under responsibility of the Bayerisches Laserzentrum GmbH

Keywords: Laser cutting; CFRP; heat conduction losses; HAZ; heat-affected zone; energy balance; carbon-fiber-reinforced plastic

* Corresponding author. Tel.: +49-7156-303-32203 ; fax: +49-7156-303-32057 .
E-mail address: patrick.mucha@de.trumpf.com

Peer-review under responsibility of the Bayerisches Laserzentrum GmbH
doi:10.1016/j.phpro.2014.08.036

Nomenclature

CFRP	carbon-fiber-reinforced plastics
c_p	mass specific heat capacity
$c_{p,\mathrm{f}}$	mass specific heat capacity of the fibers
$c_{p,\mathrm{m}}$	mass specific heat capacity of the matrix
$d_{\mathrm{k,mean}}$	measured mean width of the kerf
$d_{\mathrm{MSZ,mean}}$	measured mean width of the matrix-sublimation zone
E_{abs}	absorbed laser energy
E_{cond}	energy conducted into the sample
E_{L}	laser energy
$E_{\mathrm{not\ abs}}$	laser energy not absorbed by the sample
E_{res}	residual energy in the sample
$E_{\mathrm{s,k}}$	energy for sublimating the composite material in the kerf
$E_{\mathrm{s.m,\ MSZ}}$	energy for sublimating the matrix material in the MSZ
HAZ	heat-affected zone
h_{s}	thickness of the material
k	heat conductivity
k^*	fitted heat conductivity of the composite material describing the global heat transport
l_{c}	length of the cut
L_{s}	latent heat of sublimation
$L_{\mathrm{s,f}}$	latent heat of sublimation of the fibers
$L_{\mathrm{s,m}}$	latent heat of sublimation of the matrix
MDZ	matrix damage zone
MSZ	matrix sublimation zone
P	laser power
t	time
t_{HeatLoad}	total effective heat load time
$T_{\mathrm{Heat,1}}$	temperature in the sample for $0 < t < t_{\mathrm{HeatLoad}}$
$T_{\mathrm{Heat,2}}$	temperature in the sample for $t > t_{\mathrm{HeatLoad}}$
t_{hom}	time of homogenisation
T_{sub}	sublimation temperature
$T_{\mathrm{sub,f}}$	sublimation temperature of the fibers
$T_{\mathrm{sub,m}}$	sublimation temperature of the matrix
T_0	room temperature
T_{D}	structure damage temperature
$T_{\mathrm{D,m}}$	structure damage temperature of the matrix material
v	cutting speed
V_{f}	fiber volume fraction
w	integration variable of the error function
x	distance from the kerf wall
x'	distance from the kerf wall in the temperature distribution just after heating has stopped
y	distance in cutting direction
z	distance in direction of the laser beam propagation
ρ	density
ρ_{f}	density of the fibers
ρ_{m}	density of the matrix
ξ	argument in the error function

1. Introduction

Carbon-fiber-reinforced plastics have great potential for light weight construction due to their high strength at low density. Especially in the aerospace and automotive industry the demand for high mileage capabilities has led to a mass reduction of many parts. Therefore, respective companies try to pursue this objective by extending the range of applications for CFRP.

As tool-wear free process (Ehrenstein (2006), Caprino et al. (1996)) and non-contact operation at high cutting speeds, laser machining has been of major interest in recent investigations for example by Stock et al. (2012), Weber et al. (2013) or Crane and Brown (1981).

However, the high sublimation temperature of the fibers leads to high temperatures in and around the kerf. Together with the high heat conductivity, this leads to a large heat transport into the sample. Table 1 shows the different thermo-physical properties of the matrix material and the C-fibers, given from Haynes, CRC Handbook (2013), Sheng and Chryssolouris (1995), and Goeke and Emmelmann (2010).

Table 1. Thermo-physical properties of the CFRP components.

	Matrix	C-fiber parallel / perpendicular to fiber axis
Density ρ in kg/m³	1250	1850
Heat conductivity k in W/m K	0.2	50/5
Heat capacity c_p in J/kg K	1200	710
Latent heat of sublimation L_s in kJ/kg	1000	43000
Sublimation temperature T_{sub} in K	800	4098
Structure damage temperature T_D in K	450	3000

A specific part of the incident laser energy always flows into the material during thermal processes. This part is referred to as heat conduction losses in the following. To cut the material efficiently and fast, a process with low losses is necessary. For cutting or welding metals the heat conduction losses have already been calculated by Schultz et al. (1993), Mazumder and Steen (1980), Prusa et al. (1999) or measured by Fuerschbach (1996) in the past.

In laser machining of CFRP, the large heat transport into the sample leads to a decrease of quality in terms of a large heat-affected zone (HAZ). The formation of the HAZ was investigated for example by Abedin (2010), Weber (2011) or Jaeschke (2012). The low sublimation temperature of the matrix leads to a removal of the plastic structure within the matrix sublimation zone (MSZ). Fig. 1a) shows a cross section of a zone close to the kerf wall. The laser is depicted on the left side of the picture. It propagates in z direction and was moved in y direction for cutting the sample. The heat flows in x direction from the kerf wall into the sample. The MSZ is indicated by the dotted line. The measured mean width of the MSZ $d_{MSZ,\,mean}$ is given by the white double arrow and the dashed line.

A detail of Fig. 1a) in enlarged scale is shown in Fig. 1b). Inside the MSZ, on the left side of the picture, one can see only bare fibers and no matrix material. This proves that the matrix material was sublimated inside the MSZ. Outside the MSZ fibers and matrix material can be seen.

In a previous publication by Mucha et al. (2014) a heat flow model was used for determining the size of the visible MSZ and the matrix damage zone (MDZ, not visible in the picture). The same experimental setup and the same process parameters were used as in the present paper. A CO_2 laser “TruFlow 5000” with a maximum average power of 5 kW was used. At the used spot diameter of 150 µm the Rayleigh length was about 1 mm. The experiments were performed in ambient air without the use of additional process gases. For the experiments cuts were performed with a single-pass strategy at laser powers of 1 kW, 2 kW, and 5 kW. For each laser power the cutting speed was chosen about 5 to 10% lower than the maximum possible cutting speed to separate the material entirely. The material thickness was 2 mm. A unidirectional prepreg material with a quasi isotropic buildup sequence embedded in an epoxy matrix was used. Several thermal sensors were embedded in the material at different distances from the kerf for measuring the temperature.

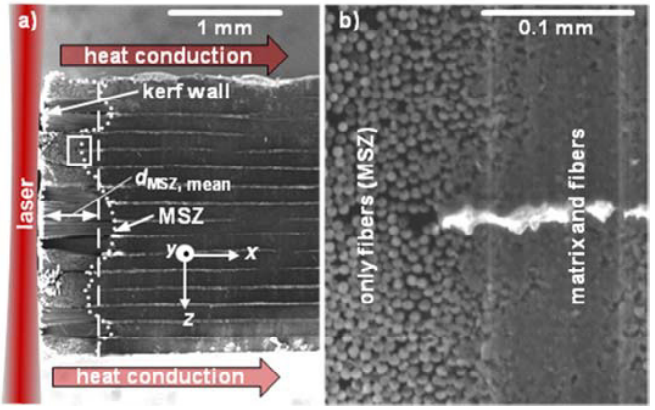

Fig. 1. SEM pictures of a cross section of a zone close to the kerf wall. a) The heat conduction from the kerf wall into the sample is symbolized by the red arrows. b) Detail of a) in enlarged scale. Within the visible MSZ nearly the total matrix material was ablated.

As mentioned above, the heat conduction losses have a large influence on the process speed and the formation of the HAZ. Therefore, in the present paper, the heat flow model and the measured temperatures were used to determine the heat conduction losses during laser cutting of CFRP. Furthermore, the energy for heating and sublimating the composite material in the kerf, the energy for heating and sublimating the matrix material in the MSZ and the energy that is not absorbed in the sample were determined using an energy balance.

2. Energy balance

The energy of the laser beam E_L applied during cutting of the samples in the experiments is given by

$$E_L = \frac{P \cdot l_c}{v}, \tag{1}$$

where P is the laser power measured at the sample, v is the cutting speed and l_c is the length of the cut. In laser cutting of CFRP the available laser energy

$$E_L = E_{abs} + E_{not\,abs} = E_{s,k} + E_{cond} + E_{not\,abs} = E_{s,k} + E_{s,m,MSZ} + E_{res} + E_{not\,abs} \tag{2}$$

can be divided into a fraction that is absorbed in the material, E_{abs}, and a fraction that is not absorbed in the material, $E_{not\,abs}$. Furthermore, the absorbed energy can be split into a fraction that is needed for the sublimation of the composite material in the kerf, $E_{s,k}$, and a fraction that is conducted into the sample, E_{cond}. The heat that flows into the sample can be further divided into a fraction that sublimates the matrix material in the MSZ, $E_{s,m,MSZ}$, and the residual heat in the sample, E_{res}. In the following, the fractions of this energy balance will be determined.

2.1. Energy for heating and sublimating the material in the kerf and the MSZ

The energy for sublimating the composite material in the kerf, $E_{v,k}$, (assuming complete sublimation) is given by

$$E_{s,k} = l_c \cdot h_s \cdot d_{k,mean} \cdot (V_f \cdot \rho_f \cdot (L_{s,f} + c_{p,f} \cdot (T_{sub,f} - T_0)) + (1 - V_f) \cdot \rho_m \cdot (L_{s,m} + c_{p,m} \cdot (T_{sub,m} - T_0))), \tag{3}$$

where h_s is the thickness of the sample, $d_{k,mean}$ is the mean width of the kerf measured at different z and y positions, V_f is the fiber volume fraction, ρ_f is the density of the fibers, ρ_m is the density of the matrix material, $L_{s,f}$ is the latent heat of the fibers, $L_{s,m}$ is the latent heat of the matrix material, $c_{p,f}$ is the heat capacity of the fibers, $c_{p,m}$ is the heat capacity of the matrix material, $T_{sub,m}$ is the sublimation temperature of the matrix material, and $T_{sub,f}$ is the sublimation temperature of the fibers.

The energy for sublimating the matrix material in the MSZ $E_{s,m,MSZ}$

$$E_{\mathrm{s,m,MSZ}} = 2 \cdot l_{\mathrm{c}} \cdot h_{\mathrm{s}} \cdot d_{\mathrm{MSZ,mean}} \cdot \rho_{\mathrm{m}} \cdot (1 - V_{\mathrm{f}}) \cdot (L_{\mathrm{s,m}} + c_{p,\mathrm{m}} \cdot (T_{\mathrm{sub,m}} - T_0)), \tag{4}$$

can be derived from the measured mean width of the MSZ d_{MSZmean} (see Fig. 1a). The existence of a MSZ on both sides of the kerf is considered by the factor 2.

2.2. Residual heat in the sample

It was shown by Mucha et al (2014) that the temperatures in the different fiber layers become identical after a certain time of homogenization $t_{\mathrm{hom}} = 3$ s (using the same setup). From this time of homogenization t_{hom} onwards, the temperature gradient in z direction was found to be approximately zero ($dT/dz \approx 0$ at $t \geq t_{\mathrm{hom}}$). The temperature gradient in y direction can be taken as $dT/dy \approx 0$ for $t \geq t_{\mathrm{hom}}$. Thus, a one-dimensional heat flow model (Carslaw and Jaeger (1959)) is used for determining the residual heat in the sample. At $t < t_{\mathrm{hom}}$ the heat conduction is not one-dimensional. The temperatures in the different fiber layers are not identical, yet. However, as the extent of the heat wave at the end of the total effective heat load time is much shorter than the extent of the heat wave of interest, i.e. after t_{hom}, one-dimensional heat flow was assumed during heating for the sake of simplicity. The process was split in two distinct phases: During the first phase, the total effective heat load time, t_{HeatLoad}, the material in the kerf is heated and sublimated. In the second phase ($t \geq t_{\mathrm{HeatLoad}}$), the material on both lateral surfaces inside the kerf cools down and the heat decays in the sample.

As seen from the material parameters in Table 1, about sixteen times more energy is needed for the sublimation of the fibers than for heating them to sublimation temperature. Therefore, the time for heating the material is much shorter than the time for sublimating the material and is neglected. In the first phase, the surface of the kerf is supposed to be at the sublimation temperature of the fibers. The one-dimensional evolution of the temperature in the sample for a constant kerf surface temperature during the effective heat load time t_{HeatLoad} is given by

$$T_{\mathrm{Heat,1}}(x,t) = (T_{\mathrm{sub,f}} - T_0) \cdot \mathrm{erfc}\left(\frac{|x|}{2\sqrt{\frac{k^* t}{\rho_{mean}\, c_{p,mean}}}} \right) + T_0, \tag{5}$$

where $T_{\mathrm{sub,f}}$ is the sublimation temperature of the fibers, T_0 is the room temperature. The mean heat conductivity k^* of the composite was assumed to describe the global heat transport into the composite material. The complementary error function erfc(ξ) is given by

$$\mathrm{erfc}(\xi) = 1 - \mathrm{erf}(\xi) = 1 - \frac{2}{\sqrt{\pi}} \int_0^{\xi} e^{-w^2} dw. \tag{6}$$

The mean density ρ_{mean}

$$\rho_{\mathrm{mean}} = \rho_{\mathrm{f}} \cdot V_{\mathrm{f}} + \rho_{\mathrm{m}} \cdot (1 - V_{\mathrm{f}}) \tag{7}$$

of the composite material is approximated with the fiber volume fraction V_{f}, the density of the matrix ρ_{m} and the fibers ρ_{f}. According to this, the mean heat capacity of the composite material $c_{p,\mathrm{mean}}$ is approximated with

$$c_{p,\mathrm{mean}} = \frac{c_{p,\mathrm{f}} \cdot \rho_{\mathrm{f}} \cdot V_{\mathrm{f}} + c_{p,\mathrm{m}} \cdot \rho_{\mathrm{m}} \cdot (1 - V_{\mathrm{f}})}{\rho_{\mathrm{f}} \cdot V_{\mathrm{f}} + \rho_{\mathrm{m}} \cdot (1 - V_{\mathrm{f}})}, \tag{8}$$

where $c_{p,\mathrm{f}}$ and $c_{p,\mathrm{m}}$ are the mass specific heat capacities of the fibers and the matrix material.

After the effective heat load time, the temperature has the distribution $T_{\mathrm{Heat},1}(x,t_{\mathrm{HeatLoad}})$. This is the initial temperature distribution for the decay of the heat wave, when heating has stopped. The undisturbed decay of the heat wave that starts at the instant of time $t = t_{\mathrm{HeatLoad}}$ is described by Carslaw and Jaeger (1959)

$$T_{\mathrm{Heat},2}(x,t) = \frac{1}{2\sqrt{\frac{\pi\, k^*}{\rho_{mean}\, c_{p,mean}}(t - t_{\mathrm{HeatLoad}})}} \int_{-\infty}^{\infty} T_{\mathrm{Heat},1}(x', t_{\mathrm{HeatLoad}}) \cdot e^{\frac{(x'-x)^2}{\frac{4\,k^*}{\rho_{mean}\, c_{p,mean}}(t - t_{\mathrm{HeatLoad}})}} dx' \tag{9}$$

for $t > t_{\mathrm{HeatLoad}}$. The coordinate in the initial temperature distribution $T_{\mathrm{Heat},1}(x',t_{\mathrm{HeatLoad}})$ was changed to x' to distinguish it from the coordinate x in the temperature distribution $T_{\mathrm{Heat},2}(x,t)$.

The residual energy in the sample E_{res} is given by the integral of the increase of the temperature $T(x)$-T_0 according to

$$E_{\mathrm{res}} = 2 \cdot \rho_{mean} \cdot c_{p,mean} \cdot l_{\mathrm{c}} \cdot h_{\mathrm{s}} \cdot \int_0^{\infty} \left(T(x) - T_0\right) dx, \tag{10}$$

where l_{c} is the length of the cut (150 mm), h_{s} is the thickness of the sample (2 mm), $T(x)$ is the temperature distribution in x direction and T_0 is the room temperature. The factor 2 represents the assumption that the heat conduction in the material on both sides of the kerf is the same.

3. Results and discussion

Determination of the temperature distribution

The temperatures in the model were fitted to temperatures measured in a sample during and just after cutting it (in the cooling phase at $t \geq t_{\mathrm{hom}}$). The mean heat conductivity k^* of the composite, which was assumed to describe the global heat transport into the composite material, and t_{HeatLoad} were used as fit parameters. The points in Fig. 2 indicate the measured increase of the temperatures ΔT in the sample at 3 s (triangles), 5 s (circles), and 10 s (crosses) after cutting a sample. The cutting speed was 7 m/min and the laser power of 2 kW. The quantities of k^* and t_{HeatLoad} in equation (9) were used to fit the experimental data in the cooling phase, i.e. at $t \geq t_{\mathrm{hom}}$. With this fit the calculations correlate very well with the measurement as seen in Fig. 2: The root mean square deviations for all curves were less than 4 K. The values of the fit parameters t_{HeatLoad} and k^* were within ±5% for all three curves. This confirms the suitability of the one dimensional approximation.

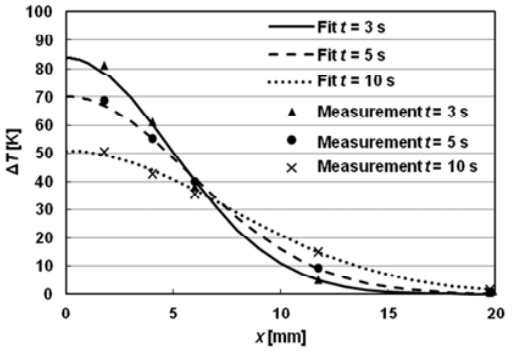

Fig. 2. Increase of temperature as a function of the distance from the kerf 3 s (triangles), 5 s (circles), 10 s (crosses) after cutting a sample. The curves represent the corresponding calculated temperature increase using the fit described in the text.

In addition, the temperature measurements and the fits were performed at laser powers of 1 kW and 5 kW and cutting speeds of 3 m/min and 20 m/min. For all these process parameters k^* was found to be 4 W/m·K ±0.1 W/m·K. This can be explained by the fact that k^* depends on the material which was identical for all experiments.

The value of the total heat load time t_{HeatLoad} varied between 1.6 ms at a cutting speed of 20 m/min (P = 5 kW) and 11 ms at a cutting speed of 3 m/min (P = 1 kW). The dependence between the process parameters and t_{HeatLoad} is discussed by Mucha et al. (2014).

Residual heat

From the temperature distributions at 3 s the amounts of residual heat were calculated using equation (10) and are shown for the investigated process parameters in Fig. 3. The error bars are resulting from the uncertainty of the fit. A change of both fit parameters in the range of 5% changes the residual heat in the range shown by the error bars (also about 5%).

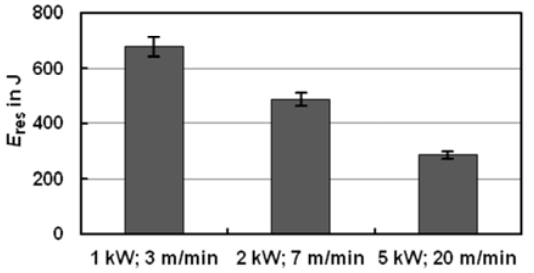

Fig. 3. Residual heat in the sample for a length of the cut of l_c = 150 mm and a thickness of the sample of h_s = 2 mm for different process parameters.

At the cutting speed of 3 m/min and a laser power of 1 kW the residual energy in the sample is 670 J. The cutting speed of 20 m/min at a laser power of 5 kW leads to a residual energy in the sample of 280 J. During the much shorter heat load time of 1.7 ms at the cutting speed of 20 m/min less heat is conducted into the material than during the heat load time of 11 ms at a cutting speed of 3 m/min.

With the constant mean heat conductivity k^* = 4 W/m·K, the temperature distribution in equation (5) is only dependent on t_{HeatLoad}. Using the temperature distribution $T(x) = T_{\mathrm{Heat,1}}(x,t_{\mathrm{HeatLoad}})$ in equation (10) E_{res} can be determined as a function of t_{HeatLoad}. The residual heat increases at increasing heat load time t_{HeatLoad}, as shown in Fig. 4.

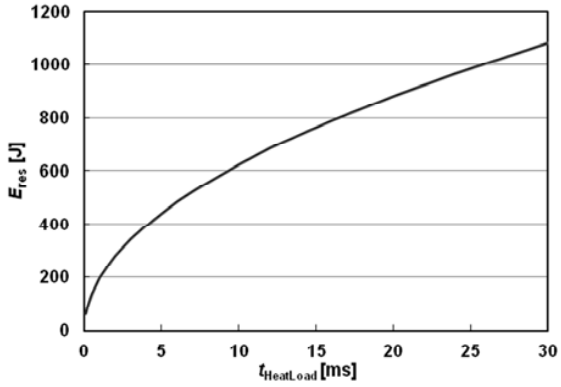

Fig. 4. Residual heat in the sample for the used sample geometry (length of the cut l_c = 150 mm; thickness of the sample h_s = 2 mm) as a function of $t_{HeatLoad}$.

Energy balance

As shown in Fig. 2, three seconds after cutting the sample the maximum temperature in the sample is about 380 K ($\Delta T \approx 85$ K). This is lower than the sublimation temperature of the matrix material. Therefore, the sublimation of the matrix material within the MSZ was already completed at the moment when temperatures in the sample were measured. The energy for sublimating the matrix material in the MSZ $E_{s,m,MSZ}$ is resulting from equation (4). It is given in Fig. 4a) for the used process parameters. For calculating $E_{s,m,MSZ}$ the mean width of the MSZ was measured. The error bars show the standard deviation of the determined values of $E_{s,m,MSZ}$. The variation of the values is resulting from the measurement of the mean width of the MSZ.

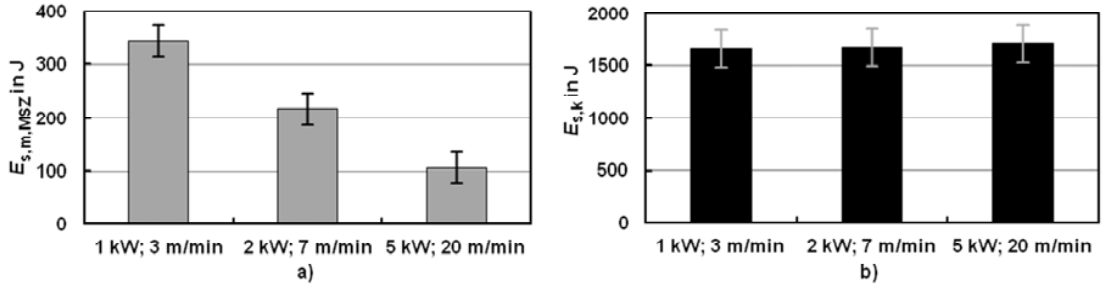

Fig. 4. a) Energy for heating and sublimating the matrix material in the MSZ for different laser powers and cutting speeds. b) Energy for heating and sublimating the composite material in the kerf for different laser powers and cutting speeds.

The mean width of the MSZ varies from 0.22 mm at v = 20 m/min and P = 5 kW up to 0.71 mm at v = 3 m/min and P = 1 kW. Therefore, the energy for sublimating the matrix material in the MSZ varies between 105 J and 340 J.

The energy for sublimating the material in the kerf $E_{s,k}$ was calculated with equation (3) and is depicted in Fig. 4b) for the used process parameters. For calculating $E_{s,k}$ the mean width of the kerf was measured. The error bars show the standard deviation of the determined values of $E_{s,k}$. The variation of the values is resulting from the measurement of the kerf width. The measured mean kerf width was found to be approximately constant for all process parameters. The volume of the sublimated material and, therefore, the energy for heating and sublimating the material in the kerf is constant at about 1700 J.

In Fig. 5 the above determined energy fractions are shown in relation to the total laser energy E_L for cutting the sample. The remaining part is the energy not absorbed by the sample as resulting from equation (2). It includes excessive energy that is transmitted through the kerf, reflected energy at the cutting front, scattered and reflected

energy in the plume, and so on. About 10% of the energy was not absorbed in the sample (white parts of the bars) in any case.

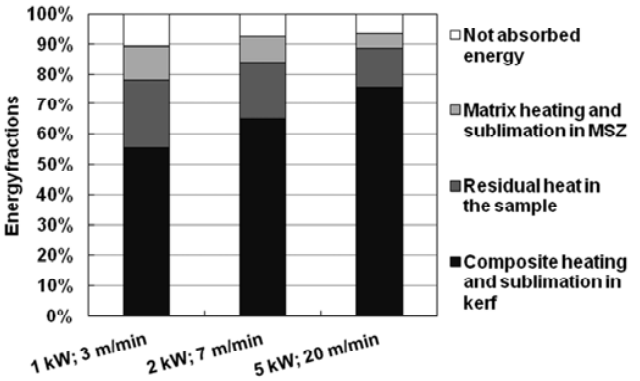

Fig. 5. Energy fractions for cutting the material for three different process parameters related to the total energy of the laser beam for cutting the sample.

At a laser power of 1 kW and a cutting speed of 3 m/min about 11% of the laser energy dissipates with the sublimated matrix material in the MSZ (light grey parts of the bars) and 23% of the total laser energy remains in the sample (dark grey parts of the bars). In total, about one third of the total laser energy is lost by heat conduction into the sample ($E_{cond} = E_{s,m,MSZ} + E_{res}$). About 55% of the total laser energy heats and sublimates the composite material in the kerf (black bars).

At increasing laser power and cutting speed the fractions of all losses decrease. The fraction for heating and sublimating the material in the kerf increases to 75% at a laser power of 5 kW. This implies that the process efficiency increases at increasing cutting speed and laser power. The reduced losses explain the disproportional increase of the maximum cutting speed at increasing laser power ($v = 3$ m/min at $P = 1$ kW compared to $v = 20$ m/min at $P = 5$ kW). At the same time the reduced fraction of the heat conduction losses at high laser powers and cutting speeds causes a smaller MSZ. However, for realizing short heat-load times in a single pass strategy, high average powers are needed.

4. Conclusion

Investigations on an energy balance in laser cutting CFRP were shown. The heat conduction losses were determined by fitting experimental data with temperatures calculated with a one-dimensional heat flow model. The heat conduction losses were found to be dominated by the effective heat-load time of the laser with a single point in the kerf. The heat conduction losses were found to decrease at increasing cutting speed and laser power. Furthermore, the energy for sublimating the matrix material in the matrix sublimation zone and the energy for sublimating the composite material in the kerf were determined. The experiments showed that about one third of the laser energy was lost by heat conduction into the material at the lowest laser power of 1 kW and a cutting speed of 3 m/min. About 11% of the laser energy dissipated with the sublimated matrix material in the MSZ and 23% of the total laser energy remained in the sample. At the highest laser power of 5 kW and a cutting speed of 20 m/min heat conduction losses of 18% were found. About 5% of the laser energy dissipated with the sublimated matrix material in the MSZ and 13% of the total laser energy remained in the sample. The reduced heat conduction losses into the sample lead to both, smaller matrix sublimation zones and a disproportional increase of the maximum possible cutting speed to separate the material entirely. Therefore, high average laser powers lead to an increase in productivity and a higher quality in terms of smaller matrix sublimation zones.

Acknowledgements

This research and development project is funded by the German Federal Ministry of Education and Research (BMBF) within the Framework Concept ”Research for Tomorrow’s Production” (FlexiCut, 02PJ2207) and managed by the Project Management Agency Karlsruhe (PTKA). The authors are responsible for the contents of this publication.

References

G. W. Ehrenstein, 2006. Faserverbund-Kunststoffe, Werkstoffe – Verarbeitung – Eigenschaften. Hanser.

G. Caprino, I. De Iorio, L. Nele, L. Santo, 1996. Effect of tool wear on cutting forces in the orthogonal cutting of UD GFRP. Composites, Part A, Appl. Sci. Manuf. 27A, 409–415.

J. Stock, M.F. Zaeh, M. Conrad, 2012. Remote Laser Cutting of CFRP: Improvements in the cut surface. Physics Procedia 39, pp. 161-170.

R. Weber, V. Onuseit, S. Tscheulin, T. Graf, 2013. High-Efficiency Laser Processing of CFRP. ICALEO 2013, Paper 1901.

K.C.A. Crane, JR Brown, 1981. Laser-induced ablation of fibre/epoxy composites. J. Phys. D: Appl. Phys., 14, pp. 2341-2349.

W. M. Haynes, 2013. CRC Handbook of Chemistry and Physics. 94th Edition, Taylor and Francis.

C. Sheng, G. Chryssolouris, 1995. Theoretical Model of Laser Grooving for Composite Materials. Journal of Composite Materials,29, pp. 96-112.

A. Goeke, C. Emmelmann, 2010. Influence of Laser Cutting Parameters on CFRP Part Quality, Physics Procedia, 5, pp. 253-258.

W. Schulz, D. Becker, J. Franke, R. Kemmerling and G. Herziger, 1993. Heat conduction losses in laser cutting of metals. J. Phys. D: Appl. Phys. 26 1357.

J. Mazumder, W.M. Steen, 1980. Heat transfer model for cw laser material processing. Journal of Applied Physics, 51(2), pp. 941-947.

J. M. Prusa, G. Venkitachalam, P.A. Molian, 1999. Esimation of heat conduction losses in laser cutting. International Journal of Machine Tools & Manufacture 39, pp. 431–458.

P. W. Fuerschbach, 1996. Measurement and prediction of energy transfer efficiency in laser beam welding. Welding Journal, vol. 75, no1 pp. 24-34.

F. Abedin, 2010. Review on Heat Affected Zone (HAZ) in Laser Machining. Proceedings of the 6th Annual GRASP Symposium, Wichita State University.

R. Weber, M. Hafner, A. Michalowski, T. Graf, 2011. Minimum damage in CFRP laser processing. Physics Proceedia 12(2), pp. 302-307.

P. Jaeschke, M. Kern, U. Stute, D. Kracht, H. Haferkamp, 2012. Laser processing of continuous carbon fibre reinforced polyphenylene sulfide organic sheets – correlation of process parameters and reduction in static tensile strength properties. Journal of Thermoplastic Composite Materials, May 10.

P. Mucha, R. Weber, B. Sommer, N. Speker, P. Berger, T. Graf, 2014. Calibrated heat flow model for determining different heat-affected zones in laser machining of CFRP. To be published elsewhere.

H. S. Carslaw, J.C. Jaeger, 1959. Conduction of heat in solids. 2nd edition, Oxford: University Press, pp. Chap. X §10.7, IX.